C2 Domain of Protein Kinase Cα: Elucidation of the Membrane Docking Surface by Site-Directed Fluorescence and Spin Labeling†

Susy C. Kohout,‡ Senena Corbalán-García,§ Juan C. Gómez-Fernández,§ and Joseph J. Falke*,‡

Department of Chemistry and Biochemistry, University of Colorado, Boulder, Colorado 80309-0215, USA, and Departamento de Bioquimica y Biologia Molecular (A), Facultad de Veterinaria, Universidad de Murcia, Apartado de Correos 4021, E30080 Murcia, Spain

Received August 8, 2002; Revised Manuscript Received October 29, 2002

ABSTRACT: The C2 domain is a conserved signaling motif that triggers membrane docking in a Ca^{2+}-dependent manner, but the membrane docking surfaces of many C2 domains have not yet been identified. Two extreme models can be proposed for the docking of the protein kinase Cα (PKCα) C2 domain to membranes. In the parallel model, the membrane-docking surface includes the Ca^{2+} binding loops and an anion binding site on β-strands 3−4, such that the β-strands are oriented parallel to the membrane. In the perpendicular model, the docking surface is localized to the Ca^{2+} binding loops and the β-strands are oriented perpendicular to the membrane surface. The present study utilizes site-directed fluorescence and spin-labeling to map out the membrane docking surface of the PKCα C2 domain. Single cysteine residues were engineered into 18 locations scattered over all regions of the protein surface, and were used as attachment sites for spectroscopic probes. The environmentally sensitive fluorescein probe identified positions where Ca^{2+} activation or membrane docking trigger measurable fluorescence changes. Ca^{2+} binding was found to initiate a global conformational change, while membrane docking triggered the largest fluorescein environmental changes at labeling positions on the three Ca^{2+} binding loops (CBL), thereby localizing these loops to the membrane docking surface. Complementary EPR power saturation measurements were carried out using a nitroxide spin probe to determine a membrane depth parameter, Φ, for each spin-labeled mutant. Positive membrane depth parameters indicative of membrane insertion were found for three positions, all located on the Ca^{2+} binding loops: N189 on CBL 1, and both R249 and R252 on CBL 3. In addition, EPR power saturation revealed that five positions near the anion binding site are partially protected from collisions with an aqueous paramagnetic probe, indicating that the anion binding site lies at or near the surface of the headgroup layer. Together, the fluorescence and EPR results indicate that the Ca^{2+} first and third Ca^{2+} binding loops insert directly into the lipid headgroup region of the membrane, and that the anion binding site on β-strands 3−4 lies near the headgroups. The data support a model in which the β-strands are tilted toward the parallel orientation relative to the membrane surface.

The C2 domain is a conserved membrane docking motif found in numerous eukaryotic signaling proteins. The cellular functions regulated by this ubiquitous signaling domain include: (a) phosphorylation of membrane proteins, (b) production and degradation of lipid derived second messengers, (c) targeting and fusion of vesicles and membranes, (d) G protein signaling by the Ras superfamily, and (e) membrane protein ubiquitination (*1*−*3*). While sharing few sequence identities, the structural similarities between different C2 domains are extensive. All C2 domains of known structure share a canonical four β-sheet antiparallel sandwich architecture, including the C2 domains from synaptotagmin I C2A (SytIA) (*4*, *5*), synaptotagmin I C2A and C2B (SytIA and SytIB) (*6*), phospholipase Cδ (PLCδ) (*7*, *8*), cytosolic phospholipase A2 ($cPLA_2$) (*9*−*11*), protein kinase Cβ I (PKCβI) (*12*), and protein kinase Cα (PKCα) (*13*, *14*). Two different C2 domain topologies have been described, Type I and Type II, differing slightly in their β-strand connectivities (*1*, *7*). For typical C2 domains of both topologies, membrane docking requires the binding of multiple Ca^{2+} ions to three interstrand loops lying at one end of the motif.

The C2 domains studied to date can be divided into two different mechanistic classes in which the forces that drive the membrane docking are primarily electrostatic or hydrophobic, respectively. For example, electrostatic interactions dominate the docking reaction for the C2A domain of synaptotagmin I and the C2 domains of conventional PKC isoforms α, β, or γ, while the C2 domain of cytosolic phospholipase A_2 docks primarily via hydrophobic interactions (*15*−*22*). Phospholipid specificity studies support this classification since domains that use the electrostatic docking mechanism require negatively charged phospholipid headgroups such as phosphatidylserine (PS), while domains known to use the hydrophobic mechanism dock to the neutral headgroups such as zwitterionic phosphatidylcholine (PC) (*21*, *22*). Ca^{2+} binding is thought to regulate membrane

† Support provided by NIH Grant GM R01-63235 (to J.J.F.), and by DGESIC Grant PB98-0389 (to J.C.G.F.).

* To whom correspondence should be addressed. E-mail: falke@colorado.edu. Tel: (303) 492-3503. Fax: (303) 492-5894.

‡ University of Colorado.

§ Universidad de Murcia.

10.1021/bi026596f CCC: $25.00
Published on Web 01/15/2003

docking by altering the electrostatic field of the protein surface such that electrostatic docking is favored, or hydrophobic docking is permitted (*23*). In addition, in at least some membrane-bound C2 domains, the Ca^{2+} ions are directly coordinated not only by protein oxygens but also by lipid headgroup oxygens, so that the bound metal ions lie at the center of a highly specific coordination array that stabilizes the protein−membrane interface (*13*, *14*). Thus, the Ca^{2+} binding loops often play an essential role in both Ca^{2+} binding and membrane docking.

Recent studies have mapped the membrane docking sites of the $cPLA_2$ and SytIA C2 domains directly to their Ca^{2+} binding loops. A site-directed fluorescence study of the $cPLA_2$ C2 domain found the Ca^{2+} binding loops responsible for docking to the membrane and proposed that they insert into the membrane (*24*). A mutagenic study of the $cPLA_2$ C2 domain determined that residues on the Ca^{2+} binding loops are necessary for docking and are potentially involved in penetration into the membrane while other residues on the β-strands are not required (*19*). Site-directed spin labeling and EPR power saturation studies of the $cPLA_2$ C2 domain found that Ca^{2+} binding loops 1 and 3 interact directly with the membrane and insert deeply into the bilayer by as much as 15 Å (*25*, *26*). Similarly, NMR studies of the SytIA C2 domain have detected phospholipid-induced chemical shifts for residues on Ca^{2+} binding loops 2 and 3 (*27*). A mutational study found that the multiple positive charges on the Ca^{2+} binding loops are important for membrane docking and that all three Ca^{2+} ions are necessary for membrane docking (*15*). Site-directed tryptophan mutagenesis and fluorescence quenching studies have identified two Phe residues in the third Ca^{2+} binding loop of the SytIA C2 domain that, when converted to Trp, insert into the membrane (*17*). Another study swapped key residues of the $cPLA_2$ and SytIA Ca^{2+} binding loops, thereby conferring the lipid preference of $cPLA_2$ C2 domain onto the SytIA C2 domain (*28*). Overall, the available evidence suggests that the membrane docking surface of C2 domains typically involves the Ca^{2+} binding loops.

The membrane docking surface of the conserved C2 domain of conventional PKC proteins has not yet been mapped out, although it is generally assumed to include the Ca^{2+} binding loops. Evidence for the involvement of these loops has been provided by the crystal structure of the PKCα C2 domain in complex with two Ca^{2+} ions and a PS headgroup analogue (*13*). In this structure, the PS headgroup phosphate directly coordinates bound Ca^{2+} and contacts the Ca^{2+} binding loops. In addition, an inorganic phosphate ion was also found in a different cleft, leading to the hypothesis that this site provides a second headgroup binding site even though it is located well outside the Ca^{2+} binding loops (*13*). A more recent crystal structure of PKCα C2 domain supports this model since a PS headgroup is observed to bind to both the Ca^{2+} binding site and the anion binding site (*14*). Figure 1A illustrates the resulting proposed parallel docking orientation of the PKCα C2 domain, in which the domain contacts the membrane via one of its two β-sheets such that the β-strands are approximately parallel to the membrane surface. This parallel orientation allows at least one Ca^{2+} binding loop and the anion binding site to directly contact the headgroup region of the membrane, and is supported by the existence of six lysines on the β-strands (*13*). Four of these lysines are proposed to interact with the PS phospholipid

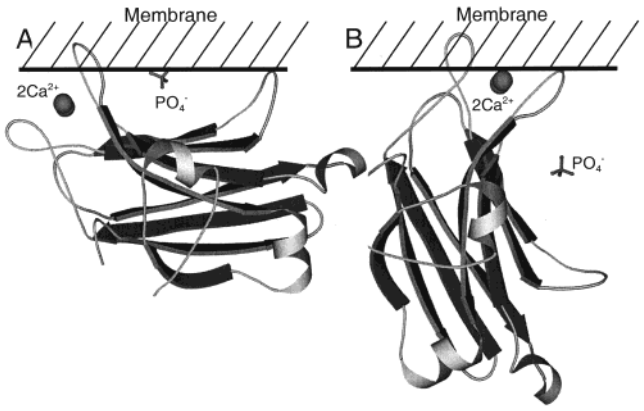

FIGURE 1: Proposed models for the docking of PKCα C2 domain to membranes. Shown are MOLSCRIPT diagrams (*43*) of the crystal structure of PKCα C2 domain (*13*) oriented according to two different hypotheses. (A) The parallel model proposes that the domain is oriented with the β-strands approximately parallel to the membrane, allowing both the Ca^{2+} binding site and a crystallographic phosphate binding site on β-strands 3−4 to interact with the lipid headgroups (*13*). (B) The perpendicular model represents the opposite extreme in which the β-strands lie perpendicular to the membrane surface and the Ca^{2+} binding site alone is responsible for docking.

headgroup (*14*). Mutation of a single lysine was found to have little effect on membrane docking, which could be argued to disfavor the parallel orientation, but this result does not rule out the parallel model since the removal of a single basic group may not be sufficiently disruptive to prevent docking (*29*). The parallel orientation of Figure 1A differs substantially from the perpendicular orientation proposed in Figure 1B, in which the β-strands have no contact with the membrane. Existing data cannot resolve whether the average orientation is parallel, perpendicular, or intermediate (tilted) relative to the membrane surface.

The present study utilizing site-directed spectroscopy (*30*) was initiated to directly map out the membrane docking face of the PKCα C2 domain and to resolve the parallel and perpendicular models for docking (Figure 1). Using site-directed mutagenesis, cysteine residues were engineered at positions scattered throughout the protein surface. These cysteines were used as attachment sites for a spin label and for a fluorophore, and the effect of each cysteine substitution, spin label attachment, and fluorophore coupling on the membrane docking affinity was determined. Subsequently, fluorescence and EPR spectroscopic studies utilized the covalently coupled fluorescein and nitroxide probes to identify positions that interact with the membrane. The combined results indicate that the Ca^{2+} binding loops insert directly into the headgroup layer of the membrane while the protein face possessing the anion binding site lies at or near the membrane surface, favoring a model in which the domain is tilted toward the parallel orientation.

METHODS AND MATERIALS

Reagents. The lipids used were 1-palmitoyl-2-oleoyl-*sn*-glycero-3-phosphocholine (phosphatidylcholine, PC) and 1-palmitoyl-2-oleoyl-*sn*-glycero-3-phosphoserine (phosphatidylserine, PS) from Avanti Polar Lipids. Fluors used were *N*-[5-(dimethylamino)-naphthalene-1-sulfonyl]-1,2-dihexadecanoyl-*sn*-glycero-3-phosphoethanolamine (dansyl-PE, dPE), *N*-(Texas Red sulfonyl)-1,2-dihexadecanoyl-sn-glycero-3-

phosphoethanolamine (Texas Red-PE, TRPE), and 5-iodoacetamide fluorescein (5-IAF) from Molecular Probes. The nitroxide spin probe used was 1-oxyl-2,2,5,5-tetramethyl-Δ^3-pyrroline-3-methyl methanethiosulfonate (MTSSL) from Toronto Research Chemicals Inc. Nickel (II) ethylenediamine-*N*,*N*′-diaacetic acid (NiEDDA) was synthesized by heating 17 mM EDDA and 17 mM $Ni(OH)_2$ in aquo to 60 °C while stirring until the solution cleared. The clear solution was incubated overnight at room temperature, and then the resulting blue solution was filtered and air-dried at 25 °C. Small unilamellar phospholipid vesicles (SUVs) were prepared by sonication with a microtip sonicator (Misonix) for 5 min at maximum power, while large unilamellar phospholipid vesicles (LUVs) were prepared by extrusion through a 100 nm membrane in a mini-extruder (Avanti Polar Lipids) as previously described (*26*, *31*). Solutions and plasticware were decalcified as described (*32*).

Protein Production. Cysteine variants were generated using two different double stranded site-directed mutagenesis methods. Initially, the Stratagene QuikChange site-directed mutagenesis kit was used following the manufacturer's protocol. Subsequently, the Roche Expand Long Template method was found to be more efficient and was used to construct the majority of mutants. Enzymes utilized in the latter procedure were a 1:1 mixture of the Roche Expand High Fidelity Polymerase and the Roche Expand Long Template Polymerase. Besides the polymerase mixture, the rest of the procedure followed the recommendations for PCR reactions included in the Roche kit. All mutagenic oligonucleotides contained the codon for cysteine as well as a silent mutation to create a restriction enzyme site (*33*). Mutant plasmids were initially identified by restriction enzyme digest and confirmed using DNA sequencing.

Purification of the cysteine variants followed the same general protocol as for the wild-type PKCα C2 domain (*13*, *22*). Briefly, the variants were expressed with a His tag and isolated using a nickel affinity column prior to proteolytic removal of the His tag by thrombin and removal of the free tag via a second nickel column as detailed previously (*22*). Two different labeling protocols were used. All steps were carried out at 25 °C unless otherwise indicated. In the first labeling protocol, following the second nickel column, the protein stock was divided in half for labeling with 5-IAF and spin label, respectively, using a protein concentration of approximately 100 μM and a 10-fold molar excess of label. Labeling reactions were done in the presence of 200 μM tris-[2-carboxymethyl]-phosphine hydrochloride (TCEP) to reduce the formation of disulfide-linked dimers. Unreacted label (~1 mM) was removed by serial dilutions via repetitive washing in a 3 mL Amicon ultrafiltration cell until the calculated concentration was less than 10 nM. In the second labeling protocol, 20 mL of cell lysate was loaded onto a 2 mL nickel column in the first affinity step of the protein purification, then the column-bound protein was labeled by addition of 80 μL of 37.9 mM spin label followed by incubation for 1 h at 25 °C. The nickel resin was thoroughly mixed every 10−15 min to ensure complete equilibration of the protein and spin label. Elution, thrombin cleavage, and the second nickel column were performed as before. Protein concentrations and purities were determined by tryptophan absorbance and SDS−PAGE gels (*34*, *35*). Labeling efficiencies were determined by running the labeled protein on an SDS−PAGE gel and measuring the ratio of the fluorescein fluorescence to the Coomassie absorbance of the relevant band before and after staining with Coomassie brilliant blue R250, respectively. Spin-labeled proteins were run on matrix-assisted laser desorption/ionization time-of-flight mass spectrometer to determine efficiency of labeling and to confirm removal of label by reduction with 5 mM DTT or 5 mM TCEP at 25 °C for 20 min.

Ligand Binding Assays. Equilibrium fluorescence experiments were carried out on a Photon Technology International QM-2000-6SE fluorescence spectrometer at 25 °C in standard assay buffer composed of 20 mM *N*-(2-hydroxyethyl)-piperazine-*N*′-2-ethanesulfonic acid (HEPES), pH 7.4 with KOH, 100 mM KCl. The excitation and emission slit widths were 4 and 8 nm for all equilibrium fluorescence experiments.

To determine the membrane affinities of the cysteine variants, as well as the fluorescein- and spin-labeled proteins, fluorescence resonance energy transfer (FRET) was used to monitor membrane docking in a phospholipid titration. For the free cysteine and spin-labeled proteins, FRET was measured between the donor, intrinsic tryptophans, and vesicles containing the acceptor, dansyl-PE. Spin-labeled C2 domain (0.5 μM) was premixed with 1 mM EDTA, 2 mM Ca^{2+} (net 1 mM free Ca^{2+}) in standard assay buffer. The free cysteine protein was generated by incubating the spin-labeled protein with 5 mM DTT for 20 min at 25 °C to reduce the spin label-Cys disulfide bond, thereby ensuring the labeled and unlabeled samples were as identical as possible. Subsequently, SUVs composed of PC/PS/dPE (72.5%:22.5%:5%) were titrated in and the protein-to-membrane FRET was monitored by the increase in dPE emission using excitation and emission wavelengths of λ_{ex} = 284 nm and λ_{em} = 520 nm, respectively. The fluorescence due to the direct excitation of the dPE was subtracted from the protein data. For the fluorescein-labeled proteins, FRET was monitored between the donor, fluorescein probe, and vesicles containing the acceptor, Texas Red-PE. Fluorescein-labeled C2 domain (0.5 μM) was premixed with 1 mM EDTA, 2 mM Ca^{2+} (net 1 mM free Ca^{2+}) and 5 mM dithiothreitol (DTT) in standard assay buffer. SUVs composed of PC/PS/TRPE (74.3%:24.7%:1%) were titrated in and the protein-to-membrane FRET was monitored from the decrease in fluorescein emission using excitation and emission wavelengths of λ_{ex} = 492 nm and λ_{em} = 520 nm, respectively. To control for the fluorescein quenching due to photodamage, the fluorescence of a separate cuvette containing labeled Ca^{2+} saturated C2 domain was subtracted from the lipid titration data following corrections for dilution. Under the conditions of this assay, the membrane affinity is approximately independent of the PS mole fraction (*22*), indicating that the affinity change that occurs as the membrane becomes loaded with C2 domains will be minor.

All ligand binding data were subjected to a nonlinear, least-squares analysis using the single independent site equation (eq 1):

$$\Delta F = \Delta F_{max}\left(\frac{x}{K_D + x}\right) \quad (1)$$

where ΔF_{max} represents the calculated maximal fluorescence change, x represents the total phospholipid concentration, and

K_D represents the apparent macroscopic equilibrium dissociation constant for lipid binding.

Effects of Ligand Binding on Fluorescein Emission. To determine the effects of Ca^{2+} and membranes on fluorescein-labeled domains, the change in fluorescein emission of labeled protein upon addition of saturating Ca^{2+} and vesicles was monitored. Specifically, fluorescein-labeled domains (~0.5 μM) were incubated in assay buffer containing 1 mM EDTA and 5 mM DTT. Saturating Ca^{2+} (2 mM), then SUVs (3:1 PC/PS or pure PC; 250−500 μM) and finally excess EDTA (10 mM) were added successively and the fluorescein emission spectra monitored after each addition (λ_{ex} = 492 nm; λ_{em}= 505−550 nm). Fluorescence changes were measured relative to the fluorescence intensity of the apo protein in the absence of Ca^{2+} and vesicles. The emission maximum at 518 nm was used when calculating the percent changes. The fluorescence change observed for pure PC membranes was subtracted out to remove the contribution due to nonspecific membrane docking.

To more closely examine the effect of membrane docking on the fluorescein probe, which possesses two titratable groups and can exist as a monoanion or dianion, the monoanion/dianion mole ratio was determined in the absence and presence of vesicles by collecting both the excitation spectrum (λ_{ex} = 400−525 nm; λ_{em} = 600 nm) and the emission spectrum (λ_{ex} = 437 nm; λ_{em} = 475−600 nm) before and after addition of SUVs. The equilibrium between monoanion and dianion shifts toward the monoanion when the fluorescein probe moves from an aqueous into a less polar or more anionic environment. The change in the monoanion/dianion mole ratio upon membrane docking was estimated from the emission spectrum using:

$$\Delta\frac{\text{monoanion}}{\text{dianion}} = \frac{\left(\frac{I_{550}}{I_{517}}\right)_{PC/PS} - \left(\frac{I_{550}}{I_{517}}\right)_{Ca^{2+}}}{\left(\frac{I_{550}}{I_{517}}\right)_{mono} - \left(\frac{I_{550}}{I_{517}}\right)_{di}} \quad (2)$$

where I_x represents the relative fluorescence emission intensity at x wavelength (monoanion peak at 550 nm and dianion peak at 517 nm), Ca^{2+} represents the intensity ratio upon addition of Ca^{2+}, PC/PS represents the intensity ratio upon addition of membranes at saturating Ca^{2+}, mono represents the intensity ratio for pure monoanion, and di represents the intensity ratio for the pure dianion (*36*). The range of this ratio change extends from zero (when the membrane-bound state exhibits the same ratio as the free Ca^{2+}-occupied protein) to unity (when the membrane-bound state is pure monoanion).

EPR Measurements. All EPR spectra were obtained on a Bruker ESP300E spectrometer equipped with a X-band loop-gap resonator (Medical Advances). For continuous wave power saturation experiments, samples were loaded into gas permeable TPX capillaries (Medical Advances) and measurements were taken as a function of the microwave power. Experiments were done at 25 °C in standard assay buffer. Spin-labeled proteins (40−100 μM) were preequilibrated with saturating Ca^{2+} (2 mM) and extruded PC/PS (3:1) LUVs (36 mM total lipid). Experiments were done in the absence or presence of paramagnetic agents which will change the relaxation rate and saturation of the resonance depending on their collision rate with the spin label. The three conditions used were equilibration with (i) nitrogen, (ii) air (containing ambient oxygen), and (iii) nitrogen in the presence of 10 mM NiEDDA. The following equation was used to fit the data to determine the best fit value of $P_{1/2}$, the microwave power required to reduce the resonance amplitude to half of its unsaturated value (*37*):

$$A = \frac{C\sqrt{P}}{\left[1 + \left(\frac{1}{2^{\epsilon}} - 1\right)\frac{P}{P_{1/2}}\right]^{\epsilon}} \quad (3)$$

where A is the first derivative peak-to-peak amplitude of the central ($m_1 = 0$) resonance, C is a scaling factor, P is the microwave power, and ϵ is a measure of the homogeneity of the saturation resonance. In this fit, C, ϵ, and $P_{1/2}$ are adjustable parameters. The best fit $P_{1/2}$ values for the oxygen-containing samples were then used to calculate the oxygen collision parameter (Π^{oxy}) using:

$$\Pi^{oxy} = \frac{P_{1/2}(O_2)/\Delta H(O_2) - P_{1/2}(N_2)/\Delta H(N_2)}{P_{1/2}(\text{DPPH})/\Delta H(\text{DPPH})} \quad (4)$$

where ΔH is the first derivative peak-to-peak line width for the central resonance. A similar equation can be written for the NiEDDA collision parameter (Π^{NiEDDA}). The $P_{1/2}$(DPPH) and ΔH(DPPH) values were obtained from a solid sample of α,α′-diphenyl-β-picrylhydrazyl (DPPH) (*38*). Finally, from the collision parameters, a membrane depth parameter, Φ, can be calculated (*37*):

$$\Phi = \ln\left[\frac{\Pi^{oxy}}{\Pi^{NiEDDA}}\right] \quad (5)$$

For those positions where only one determination of the collision and depth parameters was carried out, a general error propagation equation was used to calculate the errors (*39*).

RESULTS

Isolation of Cysteine Mutants. Site-directed mutagenesis was used to introduce 18 cysteine residues into the isolated C2 domain of PKCα which has no intrinsic cysteine residues. To minimize structural perturbations due to the labeling with the fluorescein or the spin label, the cysteine substitutions were placed at positions where the side chain β-carbon is fully solvent exposed in the crystal structure (*13*). The 18 positions chosen span all regions of the C2 domain surface. The variants were expressed in *Escherichia coli* and purified to homogeneity using a 6X-His tag which was removed via thrombin cleavage. To introduce spectroscopic probes for fluorescence and EPR, each protein preparation was divided in half and reacted with either 5-iodoacetamide fluorescein (5-IAF) or 1-oxyl-2,2,5,5-tetramethyl-Δ^3-pyrroline-3-methyl methanethiosulfonate (MTSSL) followed by removal of unreacted probe. Herein the fluorescein- and spin-labeled cysteine side chains, illustrated in Scheme 1, are abbreviated F1 and S1, respectively. Unless otherwise specified, the labeled protein was stored and all experiments were conducted in a standard buffer of 20 mM HEPES, pH 7.4, and 100 mM KCl at 25 °C.

Scheme 1

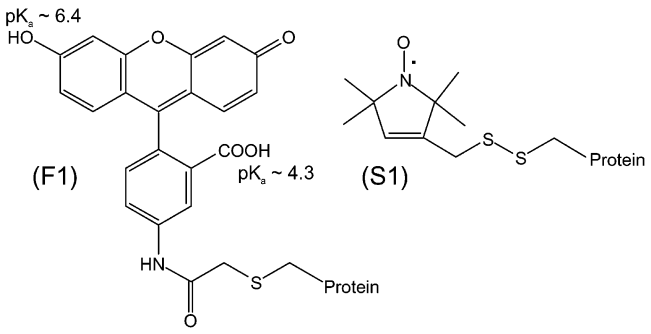

Effects of Cysteine Mutations and Probe Attachment on Membrane Affinity. Membrane docking measurements were carried out to determine the effects of the cysteine mutations and the effects of both labels on the membrane affinity of the C2 domain. Two different fluorescence resonance energy transfer (FRET) assays were used to quantitate the membrane affinities. For both the unlabeled cysteine and spin-labeled proteins, FRET was measured between the four intrinsic tryptophans of the C2 domain, which served as donors, and PC/PS/dPE (72.5%:22.5%:5%) vesicles containing a small mole fraction of dansylated phosphatidylethanolamine (dPE), which served as the acceptor. For the fluorescein-labeled proteins, FRET was measured between the protein-bound fluorescein, which served as a donor, and PC/PS/TRPE (74.3%:24.7%:1%) vesicles containing a small mole fraction of Texas Red phosphatidylethanolamine (TRPE) serving as the acceptor. Representative effects of cysteine substitution and of spin label attachment on the membrane binding of the Ca^{2+}-occupied C2 domain are illustrated in Figure 2A. As membrane is titrated into the sample containing Ca^{2+}-saturated C2 domain, the FRET signal increases until all the protein is docked.

Table 1 summarizes the apparent membrane dissociation constants, K_D, for all the modified proteins. The effects on membrane affinity are somewhat related to the size of the attached probe. At 15 of the 18 positions chosen for cysteine substitution, both the free cysteine side chain and the spin-labeled side chain have relatively small effects on membrane affinity, yielding K_D values within 3-fold of native. These small perturbations correspond to a free energy change of $\Delta\Delta G < 1\ RT$, on the order of thermal energy. At the remaining three positions, both the free cysteine side chain (K165C, H174C, and R252C) and the spin-labeled cysteine side chain (K165S1, H174S1, and R252S1) decrease membrane affinity from 3- to 6-fold, corresponding to free energy changes of $\Delta\Delta G \sim 1-2\ RT$. Coupling of the bulkier, anionic fluorescein often yields larger perturbations than the smaller, neutral spin label. At 12 of the 18 labeling positions both the free cysteine side chain and the fluorescein-labeled side chain yield membrane affinities within 3-fold of native, but at the remaining six positions fluorescein attachment decreases membrane affinity over 3-fold (M186F1, N189F1, K211F1, R216F1) or increases membrane affinity over 3-fold (K181F1, Q280F1) relative to native. The largest perturbation is a 28-fold affinity decrease observed for the fluorescein-labeled protein R216F1, which lies close to the Ca^{2+} binding site and is the only modification that changes affinity more than 6-fold. The observation that 53 of the 54 modifications alter affinity less than 6-fold, even though a subset must lie on the membrane docking surface, is consistent with the previous finding that the protein−membrane interface of C2 domains is much less sensitive to perturbation by MTSSL and fluorescein probes than a typical protein−protein interface (*24*, *26*). This unusual plasticity presumably arises from the ability of phospholipids to adjust their positions and conformations to accommodate significant side chain modifications. The small size of the perturbations suggests that the modified proteins will generally dock to the membrane with the native depth and orientation.

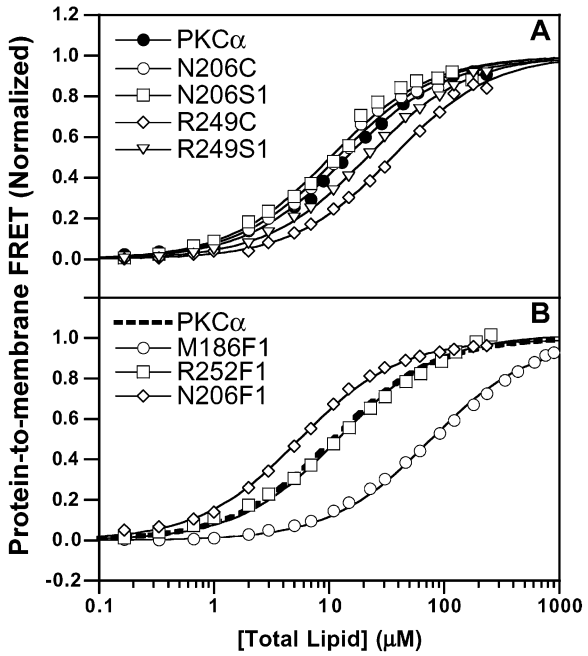

FIGURE 2: Representative membrane binding titrations for cysteine-substituted, spin-labeled (S1), and fluorescein-labeled (F1) proteins. (A) Membrane vesicles composed of PC/PS/dPE (72.5%:22.5%:5% SUVs) were titrated into a sample containing a representative Ca^{2+}-loaded protein: wild type (closed circles), N206C (open circles), N206S1 (open squares), R252C (open diamonds), or R252S1 (open upside down triangles). Protein-to-membrane FRET between the intrinsic donor Trp residues of the protein and the acceptor dansyl PE of the membrane was measured by exciting Trp while monitoring dansyl emission. (B) Membrane vesicles composed of PC/PS/TRPE (74.3%:24.7%:1% SUVs) were titrated into a sample containing a representative fluorescein-labeled Ca^{2+}-loaded protein: K230F1 (open circles), N189F1 (open squares), or R252F1 (open diamonds). Protein-to-membrane FRET between protein-bound fluorescein and membrane bound Texas Red PE was measured by exciting fluorescein while monitoring its emission decrease due to FRET. Experimental conditions for (A) and (B): 25 °C; 20 mM HEPES, pH 7.4, 100 mM KCl, 1 mM free Ca^{2+}, ~0.5 μM protein. Solid curves indicate best-fits calculated using eq 1: the best-fit apparent dissociation constants (K_D) obtained for these and other modified proteins are summarized in Table 1. The dashed curve in (B) for the wild-type C2 domain was determined using the procedure in (A).

Focusing on the nine positions where at least one modification (cysteine substitution or probe coupling) changes the membrane affinity more than 3-fold relative to wild type (Table 1), the highest density of perturbing positions is observed on the three Ca^{2+} binding loops (CBL1, CBL2, CBL3). One of the five Ca^{2+} binding loop positions yielded the large 28-fold affinity loss (R216F1), while three of these positions yielded 3- to 6-fold affinity losses (M186F1; N189S1 and F1; R252C and S1). By contrast, at the remaining 13 positions outside the Ca^{2+} binding loops, only

Table 1: Membrane Dissociation Constants (K_D) of Modified C2 Domains

mutation	location	unlabeled[b] Cys mutant	labeled with[c] MTSSL	labeled with[d] fluorescein
(wild type)		(11 ± 1) μM		
K165C	β1	63 ± 6	49 ± 5 μM	12 ± 1 μM
H174C	β2	40 ± 4	40 ± 3	4.5 ± 0.5
K181C	β2	4.5 ± 0.4	8.2 ± 0.7	1.7 ± 0.2
M186C	β2−β3 (CBL1)[a]	24 ± 1	25 ± 2	60 ± 10
N189C	β2−β3 (CBL1)	12 ± 1	3.9 ± 0.1	60 ± 10
N206C	β3−β4	12 ± 1	11 ± 1	5.4 ± 0.2
K211C	β4	16 ± 3	19 ± 1	51 ± 2
R216C	β4−β5 (CBL2)	11 ± 1	30 ± 6	310 ± 20
N224C	β5	12 ± 1	8.6 ± 0.5	12.8 ± 0.2
K230C	β5-β6	16 ± 2	16 ± 2	7 ± 1
S234C	α1	9 ± 1	7 ± 1	4.4 ± 0.7
S241C	β6	17 ± 2	14 ± 2	12.6 ± 0.3
R249C	β6−β7 (CBL3)	29 ± 5	17 ± 4	26 ± 6
R252C	β6−β7 (CBL3)	50 ± 1	35 ± 1	13.5 ± 0.4
K268C	α2	11.8 ± 0.8	11.0 ± 0.5	7.4 ± 0.3
S272C	β8	9.3 ± 0.6	8.8 ± 0.6	20 ± 3
Q280C	α3	12.5 ± 0.9	11.0 ± 0.9	3.0 ± 0.4
Y286C	C-terminus	19 ± 1	19 ± 1	10.5 ± 0.4

[a] CBL represents Ca^{2+} binding loop. [b] Apparent equilibrium dissociation constant (K_D) for C2 domain docking to 3:1 PC/PS membrane vesicles measured as illustrated in Figure 2A by protein-to-membrane FRET between intrinsic Trp (donor) and dPE (acceptor). Experimental conditions: ~0.5 μM protein, 5 mM DTT, 20 mM HEPES, pH 7.4, 100 mM KCl, 1 mM free Ca^{2+}, 72.5%:22.5%:5% PC/PS/dPE, 25 °C. [c] Same as footnote b except that DTT was omitted from experimental conditions. [d] K_D for docking to 3:1 PC/PS membrane vesicles measured as illustrated in Figure 2B by protein-to-membrane FRET between the fluorescein label (donor) and TRPE (acceptor). Experimental conditions: same as footnote b except membranes were PC/PS/TRPE 74.3%:24.7%:1%. All errors are ± SD as determined by nonlinear best fit of eq 1 to titrations possessing at least 17 data points.

five scattered across the protein surface yield membrane affinity changes as much as 3−6-fold when modified (Table 1). The high density of Ca^{2+} binding loop modifications that perturb membrane docking is consistent with previous studies of other C2 domains indicating that these loops not only bind Ca^{2+}, but also make the majority of direct protein-membrane contacts (*15*, *17*, *19*, *24*−*28*, *40*). However, Ca^{2+} and membrane binding to the PKCα C2 domain are tightly coupled (*22*); thus, the membrane affinity losses triggered by modification of the Ca^{2+} binding loops could in principle arise from loss of Ca^{2+} affinity, rather than from direct perturbation of the protein−membrane interface. The five positions where membrane affinity changes are observed outside the Ca^{2+} binding loops add further ambiguity. It follows that the pattern of membrane affinity changes triggered by surface modifications does not conclusively localize the membrane docking site. To better map out this functionally critical surface, the fluorescein- and spin-labeled proteins were used in spectroscopic studies designed to detect changes in probe environment upon Ca^{2+} binding and membrane docking.

Fluorescence Analysis of the Ca^{2+}-Triggered Conformational Change. The fluorescence intensity of fluorescein, which is strongly modulated by its protonation state, is sensitive to local environmental conditions including changes in pH and dielectric constant (*36*, *41*). To identify regions of the C2 domain involved in a Ca^{2+}-triggered conformational change, the effect of Ca^{2+} on the fluorescein emission of each protein was determined in the absence of membranes. Representative results for three fluorescein-labeled proteins are shown in Figure 3, and Table 2 summarizes the emission changes for all 18 proteins. At seven labeling positions, Ca^{2+} addition has a minimal affect on the fluorescein emission, yielding changes no larger than 20% (see K165F1 in Figure 3). However, at nine positions, a significant 20−40% fluorescein emission decrease is observed upon Ca^{2+} addition (K165F1, H174F1, M186F1, N189F1, N206F1, K230F1, S234F1, K268F1, Y286F1). Ca^{2+} binding has the most dramatic effect on positions K211F1 and R216F1 where a 70−90% fluorescein emission increase is observed (see K211F1 in Figure 3). Notably, the effect of Ca^{2+} binding to the C2 domain is well dispersed over the majority of the domain. The simplest explanation for these findings is that the Ca^{2+}-triggered conformational change is global rather than local.

Fluorescence Analysis of the Membrane Docking Surface. To identify label positions located on the membrane docking surface, membranes were added to the Ca^{2+}-occupied protein and the effect on fluorescein emission was measured. The results are summarized for representative mutants in Figure 3 and the entire set in Table 2. For nine proteins, addition of PC/PS vesicles (3:1) has a minimal effect, changing the fluorescein emission by no more than 20%. For six proteins, an intermediate 20−30% fluorescein emission decrease is observed, while for the remaining three proteins a greater than 40% emission loss is detected. A decrease in fluorescence emission intensity is consistent with, but does not prove, a transfer of the probe into a less polar or more anionic environment (*36*). Notably, the three largest emission decreases all occur at label positions on the second and third Ca^{2+} binding loops (R216F1, R249F1, R252F1), suggesting that these loops are involved in the protein−membrane docking interface. The six intermediate emission decreases are observed for two label positions on the first Ca^{2+} binding loop (M186F1, N189F1), and for four positions on the face of the protein possessing the anion binding site (N206F1, K211F1, K230F1, S234F1).

The excitation and emission spectra of fluorescein both undergo characteristic wavelength shifts when its protonation state is altered, and these spectral changes provide a sensitive detector of environmental changes. Scheme 1 above illustrates the two titratable groups associated with the aromatic system. In an aqueous environment at neutral pH, fluorescein exists predominantly as a dianion, while in a less

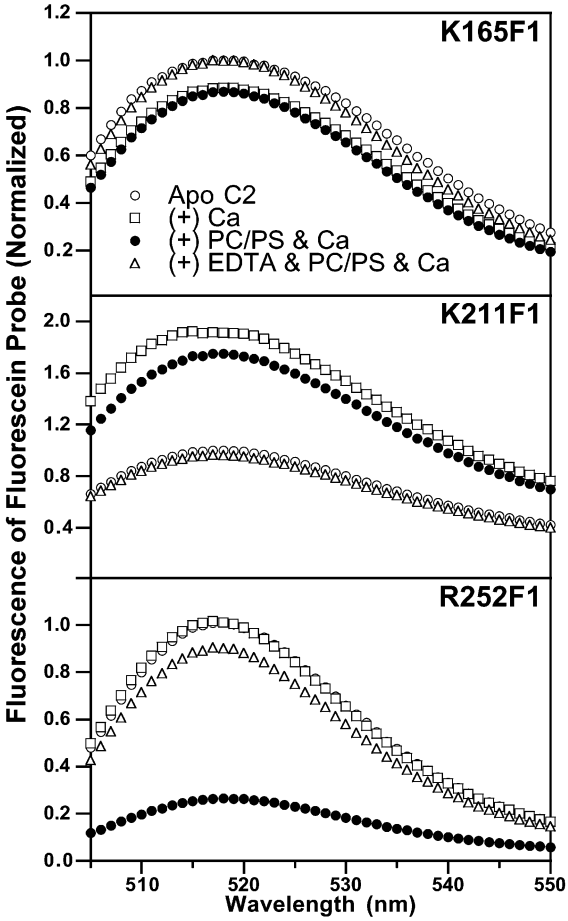

FIGURE 3: Fluorescein (F1) emission intensity changes triggered in representative proteins by Ca^{2+} binding and membrane docking. Shown is the fluorescence emission spectrum of each fluorescein-labeled apo protein (open circles), as well as spectra generated by successive addition of saturating Ca^{2+} (2 mM, open squares), then membrane vesicles (3:1 PC/PS SUVs, 250−500 μM total lipid, closed circles), and finally excess EDTA (10 mM, open triangles). For each fluorescein-labeled protein, the emission spectrum of the apo protein was used to normalize the other spectra generated. Experimental conditions: 25 °C; 20 mM HEPES, pH 7.4, 100 mM KCl, 5 mM DTT, ~0.5 μM protein. Ca^{2+}- and membrane-triggered fluorescein intensity changes are summarized in Table 2 for these and other fluorescein-labeled proteins.

Table 2: Fluorescein Emission Changes

fluorescein labeling site	location	Δ emission[a] upon addition of		Δ mono/dianion[b] ratio upon addition of PC/PS
		Ca^{2+}	PC/PS	
K165C	β1	−25 ± 9%	−3 ± 1%	2.2 ± 0.7%
H174C	β2	−22 ± 1%	−1 ± 1%	2.3 ± 0.1%
K181C	β2	−8 ± 2%	−5 ± 3%	1.2 ± 0.5%
M186C	β2−β3 (CBL1)	−35 ± 5%	−20 ± 3%	37 ± 4%
N189C	β2−β3 (CBL1)	−43 ± 3%	−23 ± 2%	45 ± 3%
N206C	β3−β4	−29 ± 1%	−22 ± 2%	17.1 ± 0.3%
K211C	β4	90 ± 10%	−30 ± 4%	7.9 ± 0.5%
R216C	β4−β5 (CBL2)	71 ± 3%	−49 ± 4%	10 ± 1%
N224C	β5	−12 ± 2%	−3 ± 1%	3 ± 1%
K230C	β5-β6	−33 ± 2%	−22 ± 2%	27 ± 2%
S234C	α1	−29 ± 9%	−24 ± 3%	4 ± 2%
S241C	β6	−8 ± 2%	−4 ± 2%	4.5 ± 0.7%
R249C	β6−β7 (CBL3)	−6 ± 1%	−60 ± 10%	36 ± 2%
R252C	β6−β7 (CBL3)	−15 ± 1%	−67 ± 7%	37 ± 1%
K268C	α2	−24 ± 1%	−2 ± 1%	0.6 ± 0.2%
S272C	β8	−18 ± 2%	−3 ± 1%	5 ± 1%
Q280C	α3	−18 ± 1%	−7 ± 2%	7 ± 1%
Y286C	C-terminus	−36 ± 5%	−15 ± 2%	4 ± 1%

[a] Fluorescein emission change upon addition of saturating Ca^{2+} (2 mM), or of saturating Ca^{2+} and membrane vesicles (3:1 PC/PS, total lipid 250 μM or 500 μM for R216C) as illustrated in Figure 3. Experimental conditions: ~0.5 μM protein, 5 mM DTT, 20 mM HEPES, pH 7.4, 100 mM KCl, 25 °C. To control for nonspecific effects of membrane addition including scattering of excitation light, the effect of addition of PC membranes which do not bind the domain was subtracted from all samples. [b] Percent increase of the fluorescein [monoanion]/[dianion] ratio upon addition of membrane vesicles (3:1 PC/PS, total lipid 250 μM or 500 μM for R216C) in the presence of saturating Ca^{2+} (2 mM) as illustrated in Figure 4 and calculated by Equation 2. Experimental conditions same as footnote a. All errors are ± SEM for $n > 3$.

polar or more anionic environment the monoanion is more prevalent. The dianion has different excitation and emission maxima, as well as a higher quantum yield, than the monoanion (*36*). Thus, the interaction of the probe with a membrane, which shifts the equilibrium toward the monoanion, triggers large spectral shifts.

Figure 4 illustrates the effects of membrane addition on the excitation and emission spectra of the fluorescein-labeled, Ca^{2+}-occupied protein. No significant effects are observed for the K165F1 protein (Figure 4, upper), while characteristic wavelength and intensity changes are observed for the R252F1 protein (Figure 4, lower) indicating conversion of dianion to monoanion. For each fluorescein-labeled protein, Table 2 presents the change in the monoanion/dianion mole ratio observed when the Ca^{2+}-saturated protein docks to the membrane. The ratio change is scaled such that 0% represents no change upon membrane docking, while 100% indicates that the fluorescein is converted completely to monoanion upon membrane docking. Table 2 indicates that 12 proteins exhibit no significant change (≤ 10%) in the monoanion/dianion ratio upon docking; thus, the majority of labeling sites do not exhibit detectable interactions with the membrane. Two proteins exhibit intermediate (15−30%) increases in the monoanion/dianion ratio, while four proteins exhibit large (35−45%) increases in this ratio upon docking (Figure 4, lower). The four fluorescein positions that exhibit the largest effects are localized to the first and third Ca^{2+} binding loops (M186F1, N189F1, R249F1, R252F1), while the two intermediate effects are observed on the face of the protein possessing the anion binding site (N206F1, K230F1). These results, together with the largest emission intensity changes noted above, suggest that the three Ca^{2+} binding loops dominate the membrane docking surface and that the face of the protein possessing the anion binding site may interact weakly with the membrane. However, the fluorescein probe could detect a long-range conformational change, or its large size could allow it to project from the protein surface through the aqueous phase to contact the surface of the membrane. It follows that the fluorescence approach could overestimate the area of the membrane docking surface. Thus, a complementary EPR approach was used to generate an independent map of the docking surface.

EPR Analysis of the Membrane Docking Surface. To further analyze the location of the membrane-docking surface, EPR measurements were carried out to identify positions that interact directly with the membrane. The approach analyzed the relative rates at which a spin label coupled to the protein collides with two other paramagnetic probes: the apolar dioxygen molecule (O_2) found predomi-

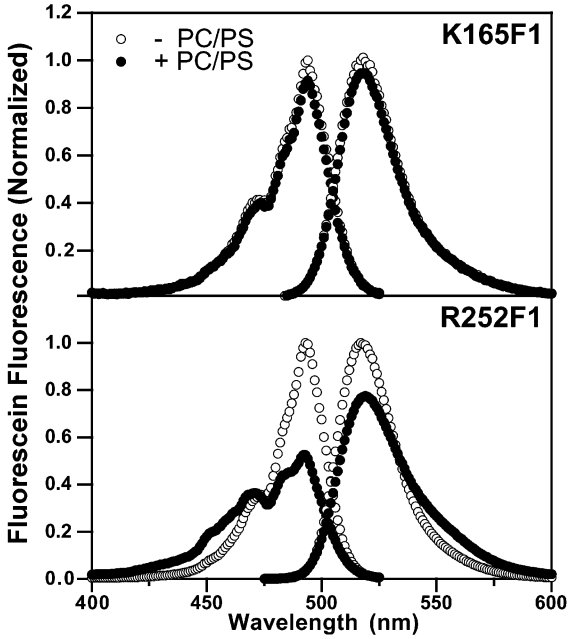

FIGURE 4: Fluorescein protonation state changes triggered by membrane docking. Shown are excitation and emission spectra of fluorescein-labeled (F1) proteins measured in the absence (open circles) and presence (closed circles) of membrane vesicles (3:1 PC/PS SUVs, 250−500 μM total lipid). Spectra were normalized to the maximum fluorescence before the addition of vesicles. For the excitation spectra, $\lambda_{em} = 600$ nm and for the emission spectra, $\lambda_{ex} = 437$ nm. The presence of the monoanion is indicated by the excitation shoulder at 470 nm and the emission shoulder at 550 nm. Experimental conditions: 25 °C, 20 mM HEPES, pH 7.4, 100 mM KCl, 5 mM DTT, 1 mM free Ca^{2+}, ~0.5 μM protein.

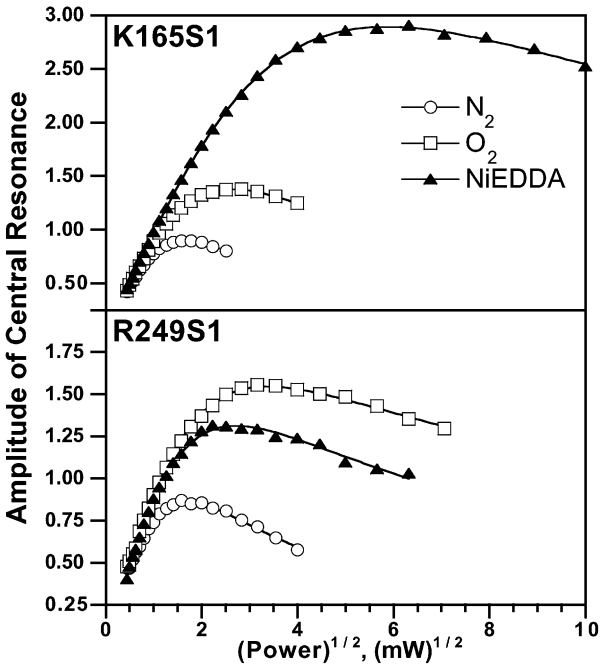

FIGURE 5: EPR power saturation of spin-labeled (S1) proteins to determine solvent and membrane exposure. Spin-labeled proteins were preequilibrated with saturating Ca^{2+} and 3:1 PC/PS vesicles to drive membrane docking. Subsequently, the indicated EPR power saturation curves were obtained by increasing the cavity microwave power while measuring the first derivative peak-to-peak amplitude change of the central resonance ($m_1 = 0$) under three differing conditions: equilibrated with N_2 (open circles), equilibrated with ambient O_2 (open squares), or equilibrated with N_2 and NiEDDA (closed triangles). Experimental conditions: 25 °C; 20 mM HEPES, pH 7.4, 100 mM KCl, 2 mM Ca^{2+}, 3:1 PC/PS LUVs at 36 mM total lipid, ~40−100 μM protein.

nantly in the membrane and the zwitterionic NiEDDA complex found primarily in the aqueous phase. EPR power saturation experiments were carried out as illustrated in Figure 5 to measure the O_2 and NiEDDA collision parameters Π^{oxy} and Π^{NiEDDA}, respectively, which were in turn used to calculate the membrane depth parameter $\Phi = \ln(\Pi^{oxy}/\Pi^{NiEDDA})$. Positive values of the depth parameter are associated with membrane penetration, while negative values indicate exposure to aqueous solution (*26*, *37*).

Table 3 summarizes the results of the power saturation measurements for the 18 proteins, including their O_2 and NiEDDA collision parameters and their membrane depth parameters. The measured Π^{oxy} collision parameters range from 0.15 to 0.38, and three of the four largest values are observed for positions on the first and third Ca^{2+} binding loops (N189S1, R249S1, R252S1), indicating that these loops exhibit high collision rates with O_2 from the membrane-associated pool. The remaining large Π^{oxy} value is observed for a position at the opposite end of the protein (K268S1); this position may lie near an O_2 binding site in the protein interior. The Π^{NiEDDA} collision parameters range from 0.11 to 1.76, a 16-fold difference, indicating that a broader range of collision rates was observed for NiEDDA than for O_2. The three lowest Π^{NiEDDA} values (0.1 to 0.3) are observed for the same three positions on the first and third Ca^{2+} binding loops that exhibited high Π^{oxy} values (N189S1, R249S1, R252S1), providing strong evidence that these loops are associated with the membrane where they collide rapidly with O_2 and are protected from collisions with NiEDDA. Intermediate Π^{NiEDDA} values (0.6 to 1.0) are observed for two positions on the first and second Ca^{2+} binding loops (M186S1, R216S1) and for five positions on the face possessing the anion binding site (N206S1, K211S1, S234S1, S241S1, Q280S1). The highest Π^{NiEDDA} values (1.1 to 1.8) are located at the remaining eight positions, including all five positions on the face opposite the anion binding site (K165S1, H174S1, K181S1, N224S1, S272S1). Together, these results indicate that the first and third Ca^{2+} binding loops penetrate most deeply into the membrane, and that the membrane partially shields the face possessing the anion binding site from collisions with NiEDDA.

The membrane depth parameter Φ provides the clearest picture of direct membrane insertion. Positive values of Φ were observed only for the same three positions on the first and third Ca^{2+} binding loops (N189S1, R249S1, R252S1). These positive Φ values arise both from increased exposure to membrane-dissolved O_2 and decreased exposure to aqueous NiEDDA, and are characteristic of membrane penetration. Positions N189S1 and R249S1 in the first and third Ca^{2+} binding loops exhibit the largest positive Φ values (0.8 ± 0.2 and 1.0 ± 0.1, respectively) and thus insert most deeply into the membrane. Position R252S1 in the third Ca^{2+} binding loop exhibits a smaller but still positive Φ value of (0.14 ± 0.09), suggesting that this position lies closer to the aqueous phase. The remaining 15 positions all exhibit Φ values below -1.2, indicating that these positions are partially or fully exposed to aqueous solution and do not penetrate significantly into the membrane. Together, the

Table 3: EPR Power Saturation Parameters

spin label site	location	[a]Π^{oxy}	[b]Π^{NiEDDA}	[c]Φ
K165C	β1	0.25 ± 0.04	1.49 ± 0.01	−1.77 ± 0.06
H174C	β2	0.26 ± 0.04	1.76 ± 0.01	−1.92 ± 0.07
K181C	β2	0.23 ± 0.06	1.13 ± 0.02	−1.6 ± 0.2
M186C	β2−β3 (CBL1)	0.17 ± 0.03	0.8 ± 0.1	−1.6 ± 0.2
N189C	β2−β3 (CBL1)	0.38 ± 0.01	0.17 ± 0.04	+0.8 ± 0.2
N206C	β3−β4	0.19 ± 0.01	1.0 ± 0.1	−1.7 ± 0.1
K211C	β4	0.17 ± 0.02	0.8 ± 0.1	−1.5 ± 0.3
R216C	β4−β5 (CBL2)	0.18 ± 0.04	0.84 ± 0.05	−1.6 ± 0.2
N224C	β5	0.24 ± 0.04	1.20 ± 0.01	−1.63 ± 0.09
K230C	β5−β6	0.26 ± 0.04	1.3 ± 0.1	−1.7 ± 0.2
S234C	α1	0.15 ± 0.06	0.88 ± 0.01	−1.74 ± 0.07
S241C	β6	0.22 ± 0.07	0.76 ± 0.03	−1.3 ± 0.2
R249C	β6−β7 (CBL3)	0.30 ± 0.01	0.11 ± 0.01	+1.0 ± 0.1
R252C	β6−β7 (CBL3)	0.3 ± 0.1	0.3 ± 0.1	+0.14 ± 0.09
K268C	α2	0.32 ± 0.09	1.68 ± 0.01	−1.7 ± 0.1
S272C	β8	0.28 ± 0.03	1.71 ± 0.01	−1.83 ± 0.05
Q280C	α3	0.2 ± 0.2	0.6 ± 0.1	−1.4 ± 0.3
Y286C	C-terminus	0.26 ± 0.04	1.34 ± 0.01	−1.64 ± 0.09

[a] Oxygen collision parameter (Π^{oxy}) measured in the presence of saturating Ca^{2+} (2 mM), saturating membrane vesicles (3:1 PC/PS, total lipid 36 mM), and ambient O_2. Experimental conditions: 40−100 μM protein, 20 mM HEPES, pH 7.4, 100 mM KCl, 25 °C. [b] NiEDDA collision parameter (Π^{NiEDDA}) measured in the presence of N_2, saturating Ca^{2+} (2 mM), saturating membrane vesicles (3:1 PC/PS, total lipid 36 mM), and NiEDDA (10 mM). Experimental conditions as in footnote a. [c] Membrane depth parameter calculated from the collision parameters ($\Phi = \ln[\Pi^{oxy}/\Pi^{NiEDDA}]$). Positive values indicate membrane insertion, negative values indicate exposure to aqueous solvent (*26*, *37*).

fluorescence and EPR data indicate that the Ca^{2+} binding loops serve as the primary membrane docking site with the Ca^{2+} binding loops 1 and 3 penetrating into the headgroup region of the membrane. The anion binding site on β-strands 3−4 lies at or near the surface of the headgroup region.

DISCUSSION

When Ca^{2+} binds to the C2 domain of PKCα, fluorescence emission changes are observed at 11 of 18 fluorescein labeling positions tested on the protein surface. It follows that the structural or electrostatic effects of Ca^{2+} binding are transmitted over a large fraction of the protein. The simplest explanation is that Ca^{2+} binding triggers a global conformational change through the β-strands. Previous findings for the C2A domain of synaptotagmin I have indicated that Ca^{2+} binding causes only a localized conformational change within the Ca^{2+} binding loops (*5*), suggesting that the Ca^{2+} activation mechanism of the two domains may be different. An alternative explanation for the PKCα C2 domain findings is that Ca^{2+} binding triggers a global electrostatic change transmitted across large regions of the protein surface by subtle rearrangements of exposed side chains and nearby solvent molecules. Fluorescein emission is highly sensitive to local electrostatics and pH, and can detect subtle changes. Such long-range electrostatic effects are less likely, however, since experiments were carried out at an ionic strength approaching physiological (100 mM KCl). Thus, Ca^{2+} binding probably triggers a global conformational change.

Following Ca^{2+} binding, the activated PKCα C2 domain docks to a membrane. The present findings place strong constraints on the region of the protein surface that makes direct membrane contacts. Combining the results of lipid affinity, fluorescence, and EPR measurements, a model is proposed for the membrane docking face and orientation of the PKCα C2 domain as illustrated in Figures 6 and 7. The model reflects the overall conclusion that all of the direct membrane insertions are localized to the Ca^{2+} binding loops, such that loop positions N189, R249, and R252 penetrate into the headgroup layer of the membrane. The model also proposes that the face of the domain possessing the anion binding site lies at or near the membrane surface (Figures 6 and 7). These constraints indicate that, overall, the domain is tilted with the β-strands oriented nearly parallel to the plane of the membrane (Figures 1A, 6, and 7). The following discussion analyzes the lipid affinity, fluorescence, and EPR results relevant to the membrane docking depth and orientation.

The membrane affinity changes triggered by C2 domain modifications (cysteine substitution, spin labeling, or fluorescein coupling) are summarized in Figure 6A. This approach serves as a control for the effects of spectroscopic labeling on membrane docking and, in principle, can also help identify residues involved in docking. Highlighted in Figure 6A are positions at which side chain modification alters the membrane affinity more than 3-fold. These largest membrane affinity changes are observed at nine positions scattered over most surfaces of the protein, suggesting that membrane docking involves a global conformational change that allosterically couples distant positions to the membrane docking site. The highest density of perturbed positions is observed on the three Ca^{2+} binding loops, where four of the five positions tested exhibit altered membrane affinities when the native side chain is modified. However, the five remaining perturbed positions lie outside the Ca^{2+} binding loops on different regions of the protein surface. Thus, although the membrane affinity effects are consistent with the importance of the three Ca^{2+} binding loops in membrane docking, they do not conclusively determine the location of the membrane docking face.

The results of the fluorescence analysis of membrane docking are summarized in Figure 6B, which highlights the positions where fluorescein probes exhibit the largest changes in both emission intensity and monoanion/dianion ratio. The largest membrane docking effects on emission intensity are observed for fluorescein labeling sites on Ca^{2+} binding loops two and three (R216F1, R249F1, and R252F1), where intensity decreases exceeding 40% were observed upon docking. The largest effects of docking on the fluorescein monoanion−dianion equilibrium are observed for labeling positions on the first and third Ca^{2+} binding loops (M186F1, N189F1, R249F1, and R252F1), where the monoanion/dianion ratio increased over 35% upon membrane association. Thus, the largest environmental changes triggered by membrane docking are all localized to the three Ca^{2+} binding loops, and the directions of the changes are consistent with fluorescein insertion into a less polar or more anionic membrane environment where the emission intensity decreases and the monoanion/dianion ratio increases. Besides the large effects localized to the Ca^{2+} binding loops, smaller fluorescein emission changes (20−30%) or monoanion/dianion ratio shifts (15−30%) are observed at four positions on the face possessing the anion binding site (N206F1, K211F1, K230F1, S234F1). These smaller, membrane-triggered environmental changes could indicate a more expansive membrane docking surface extending beyond the

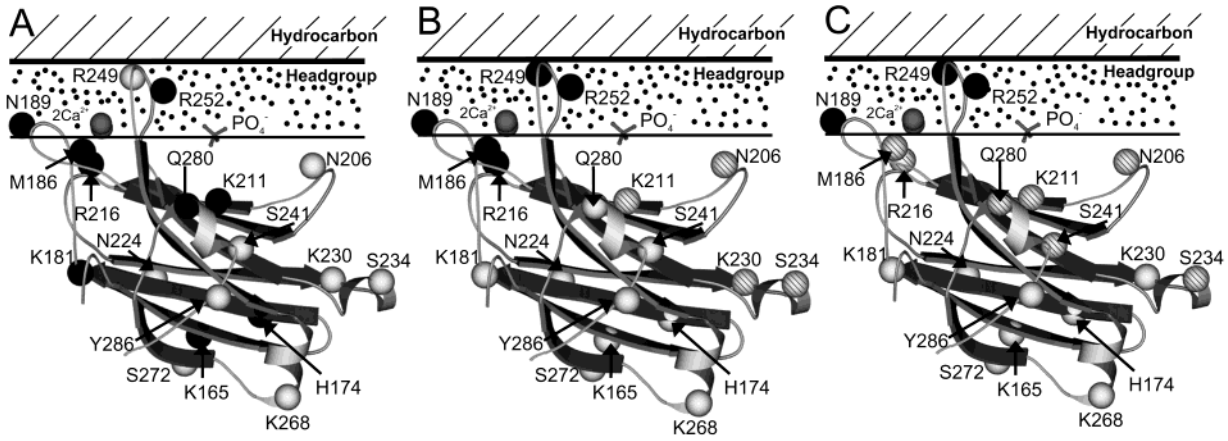

FIGURE 6: Locations of large fluorescence and EPR effects triggered by membrane docking. Shown are MOLSCRIPT (*43*) ribbon diagrams of the PKCα C2 domain crystal structure in the proposed orientation relative to the membrane headgroup and hydrocarbon layers. The diagrams indicate the positions of the 18 Cys substitutions, highlighting the positions of large membrane affinity, fluorescence or EPR changes. (A) Membrane affinity effects. Positions where cysteine-substitution, spin-label attachment, or fluorescein coupling alter the membrane docking affinity >3-fold are shown in black; other positions exhibiting little or no change are shown in gray. (B) Fluorescein emission effects. Positions where fluorescein exhibited a large emission loss (>40%) or a large gain in the monoanion/dianion mole ratio (>25%) upon membrane docking are shown in black; positions exhibiting an intermediate emission loss (20−30%) or increase in the monoanion/dianion ratio (15−30%) are hatched; other residues are shown in gray. (C) EPR power saturation effects. For each spin-labeled protein, the membrane depth parameter $\Phi = \ln(\Pi^{oxy}/\Pi^{NiEDDA})$ was determined from the ratio of collision rates for the membrane probe O_2 and the aqueous probe NiEDDA. Positions with positive Φ values indicating membrane penetration ($\Phi > 0$) are shown in black; positions exhibiting moderate protection from collisions with NiEDDA ($\Pi^{NiEDDA} = 0.6-1.0$) are hatched; other residues are shown in gray.

Ca^{2+} binding loops to include the anion binding site, or could indicate an allosteric conformational change transmitted from the membrane docking surface to distal positions. One caution with regard to the fluorescence approach is the large size of the cysteine-coupled fluorescein probe, which is considerably larger than any of the native side chains it replaces. It follows that the fluorescence approach could overestimate the size of the membrane docking surface wherever the bulky, hydrophobic fluorescein probe is able to extend from a solvent-exposed position to the surface of the membrane. Thus, it is useful to complement the information provided by fluorescence with information provided by EPR, especially since the nitroxide spin probe is significantly smaller and less perturbing than the fluorescein probe.

The findings of the EPR approach are summarized in Figure 6C, which highlights the positions that exhibit the largest spin label depth parameters (Φ) for membrane insertion. This depth parameter is determined by the relationship $\Phi = \ln(\Pi^{oxy}/\Pi^{NiEDDA})$, which is related to the ratio of spin label collisions with membrane-dissolved oxygen (Π^{oxy}) to spin label collisions with aqueous Ni-EDDA (Π^{NiEDDA}) (*26*, *37*). The results indicate that three positions on the first and third Ca^{2+} binding loops are inserted into the membrane, while the remaining positions are partially or fully exposed to aqueous solvent. Specifically, N189S1 on the first Ca^{2+} binding loop and both R249S1 and R252S1 on the third Ca^{2+} binding loop exhibit high oxygen collision rates, low Ni-EDDA collision rates, and positive depth parameters characteristic of membrane penetration (Table 3). The Φ values of N189S1 and R249S1 ($\Phi = +0.8 \pm 0.2$ and $+1.0 \pm 0.1$, respectively) are significantly larger than that of R252S1 ($\Phi = +0.14 \pm 0.09$), indicating that the latter is less deeply buried in the membrane. The depth parameter Φ can be converted into an approximate distance of membrane penetration by comparison with a previously determined standard curve relating Φ to membrane depth (*26*). Such a comparison suggests that the spin-labeled N189S1 and R249S1 side chains are inserted into the polar headgroup layer at or near the interface with the bilayer hydrocarbon core, while the spin-labeled R252S1 side chain is located in the polar headgroup layer closer to aqueous solvent. It should be noted, however, that the flexibility of the spin labeled side chain introduces uncertainty into this analysis; thus, the depth assignments are qualitative. The 15 remaining positions all exhibit highly negative depth parameters indicating partial or full solvent exposure, but seven positions exhibit low oxygen collision rates as well as partial shielding from collisions with aqueous Ni-EDDA (M186S1, N206S1, K211S1, R216S1, K234S1, S241S1, Q280S1). The simplest model places these residues outside but nearby the membrane, where they are outside the oxygen gradient of the bilayer but are sterically protected from collisions with the large Ni-EDDA complex.

Overall, the EPR results provide strong evidence that only the Ca^{2+} binding loops directly penetrate into the membrane. In the native C2 domain, the polar and charged N189, R249, and R242 side chains most likely interact with polar and anionic groups inside the headgroup layer. The results also place the anion binding site at or near the membrane surface, thereby tilting the β-strands toward a parallel orientation relative to the membrane surface as illustrated in Figure 1A. A detailed model of the proposed orientation is shown in Figure 7. This nearly parallel orientation is similar to that predicted based on the assumption that lipid headgroups dock both to the protein-bound Ca^{2+} ions and to the anion binding site (*13*, *14*). The model of Figure 7 suggests that the effects of membrane docking on fluorescein and spin label probes at the K230 and S234 positions may be transmitted allosterically through interactions with the $\beta3-\beta4$ interstrand loop, which lies significantly closer to the membrane surface than K230 and S234.

The nearly parallel membrane docking orientation observed for PKCα C2 domain is significantly different from the docking angle previously observed for the $cPLA_2$ C2

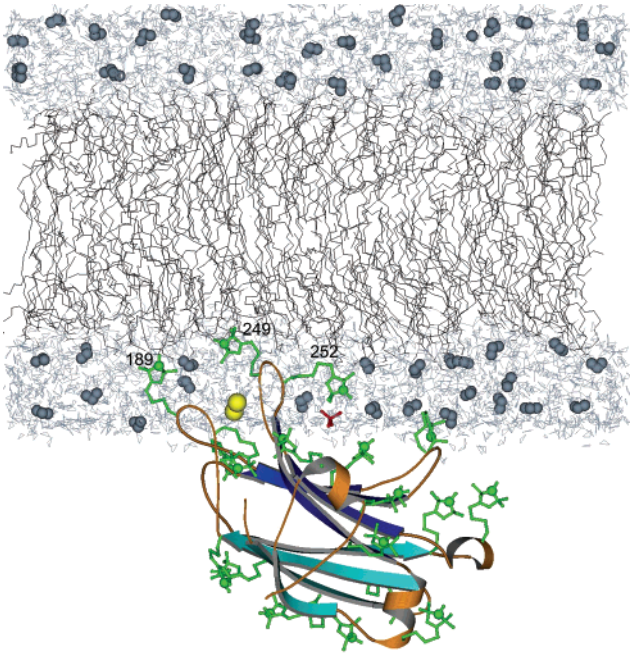

FIGURE 7: Deduced orientation of the membrane-bound PKCα C2 domain relative to the membrane surface. Shown is a model membrane of pure lipids (*44*, *45*) to which the crystal structure of the isolated PKCα C2 domain has been docked (*13*). The headgroup layers of the membrane exhibit high heavy atom densities due to the presence crystallographic waters, some of which are highlighted (small space filled molecules), while the central hydrocarbon layer exhibits a lower atom density. For each labeling site on the protein surface, a nitroxide spin label (ball-and-stick, with the nitrogen indicated by sphere) was modeled onto the crystal structure using the program INSIGHT II (Biosym Technologies). Most of the spin labels have been given the g^+, g^+ dihedral angles believed to be most common (*46*) except for those where the dihedral angles are constrained to fit the EPR data (M186S1, N189S1, N206S1, R216S1, K230S1, S234S1, R249S1, and R252S1). Also shown are two bound Ca^{2+} ions (large yellow spheres), the Ca^{2+} binding loops 1 and 3 that directly contact the membrane, and the phosphate ion (red) bound in the anion binding site on strands 3−4.

domain, which is tilted away from the parallel orientation (*19*, *24*, *26*). In both models, the three Ca^{2+} binding loops dominate the membrane docking surface with the first and third Ca^{2+} binding loops penetrating into the membrane. However, the penetration of the $cPLA_2$ C2 domain into the membrane is significantly greater since its spin-labeled side chains exhibit membrane depth parameters ranging up to $\Phi = +3.1 \pm 0.5$ (*26*) compared to an upper limit of $\Phi = +1.0 \pm 0.1$ observed thus far for the PKCα C2 domain. These contrasting penetration depths, measured under identical conditions, are consistent with the contrasting membrane-docking mechanisms of the two C2 domains (*21*, *22*): the $cPLA_2$ C2 domain docks via hydrophobic interactions with the hydrocarbon region of the membrane core, while the PKCα C2 domain interacts with negative charges in the headgroup region. Moreover, the $cPLA_2$ C2 domain lacks the anion binding site that the PKCα C2 domain possesses on strands 3−4 outside the calcium binding loops.

The nearly parallel docking orientation observed for the PKCα C2 domain in the present study (Figure 7) leaves open the possibility that the anion binding site interacts with a biologically important phosphate on a lipid headgroup as previously proposed (*13*, *14*). Under the conditions utilized herein, the site does not appear to directly penetrate into the headgroup region where it could contact a headgroup phosphate. Instead, the site may draw a lipid partially up out of the membrane to bind its headgroup, or the site may penetrate into the headgroup region only during a specific signaling state. For example, the site could be driven into the headgroup layer by the appearance of a signaling lipid to which it binds, or by signaling conformational changes triggered within other domains of the full-length PKC enzyme. Alternatively, the site could interact with a phosphorylated amino acid on a different domain of full-length PKCα, which is activated by phosphorylation (*42*), or on a different protein. Further studies will be needed to determine whether the phosphate binding site plays an important biological role.

ACKNOWLEDGMENT

The authors gratefully acknowledge Nathan Malmberg of the Falke lab for helpful discussions and assistance with EPR measurements.

SUPPORTING INFORMATION AVAILABLE

EPR spectra obtained for each of the 18 spin-labeled proteins in the apo, Ca^{2+}-occupied, and membrane-bound states are presented as Supporting Information available free of charge via the Internet at http://pubs.acs.org.

REFERENCES

1. Nalefski, E. A., and Falke, J. J. (1996) *Protein Sci. 5*, 2375−2390.
2. Rizo, J., and Sudhof, T. C. (1998) *J. Biol. Chem. 273*, 15879−15882.
3. Hurley, J. H., and Misra, S. (2000) *Annu. Rev. Biophys. Biomol. Struct. 29*, 49−79.
4. Sutton, R. B., Davletov, B. A., Berghuis, A. M., Sudhof, T. C., and Sprang, S. R. (1995) *Cell 80*, 929−938.
5. Shao, X., Fernandez, I., Sudhof, T. C., and Rizo, J. (1998) *Biochemistry 37*, 16106−16115.
6. Sutton, R. B., Ernst, J. A., and Brunger, A. T. (1999) *J. Cell Biol. 147*, 589−598.
7. Essen, L. O., Perisic, O., Cheung, R., Katan, M., and Williams, R. L. (1996) *Nature 380*, 595−602.
8. Grobler, J. A., Essen, L. O., Williams, R. L., and Hurley, J. H. (1996) *Nat. Struct. Biol. 3*, 788−795.
9. Perisic, O., Fong, S., Lynch, D. E., Bycroft, M., and Williams, R. L. (1998) *J. Biol. Chem. 273*, 1596−1604.
10. Xu, G. Y., McDonagh, T., Yu, H. A., Nalefski, E. A., Clark, J. D., and Cumming, D. A. (1998) *J. Mol. Biol. 280*, 485−500.
11. Dessen, A., Tang, J., Schmidt, H., Stahl, M., Clark, J. D., Seehra, J., and Somers, W. S. (1999) *Cell 97*, 349−360.
12. Sutton, R. B., and Sprang, S. R. (1998) *Structure 6*, 1395−1405.
13. Verdaguer, N., Corbalan-Garcia, S., Ochoa, W. F., Fita, I., and Gomez-Fernandez, J. C. (1999) *EMBO J. 18*, 6329−6338.
14. Ochoa, W. F., Corbalan-Garcia, S., Eritja, R., Rodriguez-Alfaro, J. A., Gomez-Fernandez, J. C., Fita, I., and Verdaguer, N. (2002) *J. Mol. Biol. 320*, 277−291.
15. Zhang, X., Rizo, J., and Sudhof, T. C. (1998) *Biochemistry 37*, 12395−12403.
16. Ubach, J., Zhang, X., Shao, X., Sudhof, T. C., and Rizo, J. (1998) *EMBO J. 17*, 3921−3930.
17. Chapman, E. R., and Davis, A. F. (1998) *J. Biol. Chem. 273*, 13995−14001.
18. Nalefski, E. A., McDonagh, T., Somers, W., Seehra, J., Falke, J. J., and Clark, J. D. (1998) *J. Biol. Chem. 273*, 1365−1372.
19. Bittova, L., Sumandea, M., and Cho, W. (1999) *J. Biol. Chem. 274*, 9665−9672.
20. Perisic, O., Paterson, H. F., Mosedale, G., Lara-Gonzalez, S., and Williams, R. L. (1999) *J. Biol. Chem. 274*, 14979−14987.
21. Nalefski, E. A., Wisner, M. A., Chen, J. Z., Sprang, S. R., Fukuda, M., Mikoshiba, K., and Falke, J. J. (2001) *Biochemistry 40*, 3089−3100.

22. Kohout, S. C., Corbalan-Garcia, S., Torrecillas, A., Gomez-Fernandez, J. C., and Falke, J. J. (2002) *Biochemistry 41*, 11411−11424.
23. Murray, D., and Honig, B. (2002) *Mol. Cell 9*, 145−154.
24. Nalefski, E. A., and Falke, J. J. (1998) *Biochemistry 37*, 17642−17650.
25. Ball, A., Nielsen, R., Gelb, M. H., and Robinson, B. H. (1999) *Proc. Natl. Acad. Sci. U.S.A. 96*, 6637−6642.
26. Frazier, A. A., Wisner, M. A., Malmberg, N. J., Victor, K. G., Fanucci, G. E., Nalefski, E. A., Falke, J. J., and Cafiso, D. S. (2002) *Biochemistry 41*, 6282−6292.
27. Chae, Y. K., Abildgaard, F., Chapman, E. R., and Markley, J. L. (1998) *J. Biol. Chem. 273*, 25659−25663.
28. Gerber, S. H., Rizo, J., and Sudhof, T. C. (2002) *Diabetes 51 Suppl. 1*, S12−18.
29. Conesa-Zamora, P., Lopez-Andreo, M. J., Gomez-Fernandez, J. C., and Corbalan-Garcia, S. (2001) *Biochemistry 40*, 13898−13905.
30. Falke, J. J., Sternberg, D. E., and Koshland, D. E. (1986) *Biophys. J. 49*, 20a.
31. Nalefski, E. A., Slazas, M. M., and Falke, J. J. (1997) *Biochemistry 36*, 12011−12018.
32. Needham, J. V., Chen, T. Y., and Falke, J. J. (1993) *Biochemistry 32*, 3363−3367.
33. Nalefski, E. A., Shaw, K. T., and Rao, A. (1995) *J. Biol. Chem. 270*, 22351−22360.
34. Gill, S. C., and von Hippel, P. H. (1989) *Anal. Biochem. 182*, 319−326.
35. Laemmli, U. K. (1970) *Nature 227*, 680−685.
36. Sjoback, R., Nygren, J., and Kubista, M. (1995) *Spectrochim. Acta Part A 51*, L7−L21.
37. Altenbach, C., Greenhalgh, D. A., Khorana, H. G., and Hubbell, W. L. (1994) *Proc. Natl. Acad. Sci. U.S.A. 91*, 1667−1671.
38. Farahbakhsh, Z. T., Altenbach, C., and Hubbell, W. L. (1992) *Photochem. Photobiol. 56*, 1019−1033.
39. Taylor, J. R. (1982) *An Introduction to Error Analysis: The study of uncertainities in physical measurements*, 2nd ed., University Science Books, Sausalito, CA.
40. Medkova, M., and Cho, W. (1998) *J. Biol. Chem. 273*, 17544−17552.
41. Stanton, S. G., Kantor, A. B., Petrossian, A., and Owicki, J. C. (1984) *Biochim. Biophys. Acta 776*, 228−236.
42. Newton, A. C. (2001) *Chem. Rev. 101*, 2353−2364.
43. Kraulis, P. J. (1991) *J. Appl. Crystallogr. 24*, 946.
44. Heller, H., Schaefer, M., and Schulten, K. (1993) *J. Phys. Chem. 97*, 8343−8360.
45. Heller, H. (1993) Technical University of Munich, Munich, Germany.
46. Langen, R., Oh, K. J., Cascio, D., and Hubbell, W. L. (2000) *Biochemistry 39*, 8396−8405.

BI026596F